Shapelets and Related Techniques in Radio-Astronomical Imaging

Sarod Yatawatta
Kapteyn Institute, University of Groningen,
and ASTRON,
The Netherlands.
yatawatta@astron.nl

Abstract

We present the use of orthonormal basis functions, in particular, shapelets and prolate spheroidal wave functions, in radio astronomical imaging. By using such methods, it is possible to overcome some limitations of traditional pixel based image deconvolution. Therefore, such techniques will enable us to increase the achievable imaging dynamic range thus paving the way for novel scientific results. We give an overview of the current state of the art of such methods and provide examples of its use.

I. Introduction

Even though any extended radio source could be represented by a set of delta functions [1], in practice this is difficult due to finite resolution and noise. We have shown [2] that this is indeed a problem especially for the case when we have partially resolved sources. Thus, traditional pixel based CLEAN [3] algorithms (where the basis functions are a set of pixels) fail to perform satisfactorily, limiting the dynamic range when we have bright extended sources. Although it is possible to extend CLEAN with pixels of different scale [4], in this paper we propose the use of orthonormal basis functions, such as shapelets [5], [6] or prolate spheroidal wave functions [7], [8].

Before we proceed, we shall revisit some well known concepts in radio astronomical imaging, i.e., *image fidelity* and *dynamic range*. The dynamic range is widely defined as the ratio between the peak intensity and the noise floor. However, there are many definitions for fidelity, mostly derived from the difference of the observed image from the true image [9]. Therefore, without the knowledge of the true image, it is hard to measure image fidelity. We shall therefore refine our definition of image fidelity using information theory, based on the Landau-Pollak theorem [8], [10].

In its simplest form, Landau-Pollak theorem (applicable to radio astronomical imaging) states that the number of degrees of freedom of any given source (N) could be no greater than the product of the area of the image (A_{lm}) and the area of the source observed in the Fourier plane (A_{uv}). The area of a given source in the image plane is limited by the noise floor. On the other hand, the area on the Fourier plane is given by the uv coverage. The uv coverage is determined by the duration of the observation and the bandwidth of the observation. However, when we have a completely filled uv plane, A_{uv} is determined by the area of the Fourier transform of the source.

It should be noted that the noise floor is not only determined by the system noise. As studied in [12], calibration errors as well as confusion, raise the noise floor. Therefore, the only way to lower the noise floor is to minimize calibration errors and confusion (because the receiver noise is fixed). For this we need to improve our sky model and source models, thus increasing the fidelity of our source models. Hence, by the repetition of updating sky/source models and self-calibration, we increase both the dynamic range as well as image fidelity. Thus we see a complex relationship between image fidelity and dynamic range as shown in Fig. 1. In Fig. 1, we start from an initial sky model and uncalibrated data. After each calibration, we update the sky model. Therefore, at each of these stages, we increase the dynamic range and fidelity, until we reach the theoretical limits.

One could wonder the relationship between Fig. 1 and the topic of this paper. We would like to emphasize two major points. First, in order to perform self calibration, it is essential to use basis functions that have simple relationships between the image and Fourier planes. Shapelets (Cartesian) satisfy this criterion. Secondly, in the case where we have poor uv coverage, thus small A_{uv} and hence, poor fidelity, we could still achieve the full dynamic range. This implies that even if we have partially resolved source (hence poor fidelity), we could still produce high dynamic range images. Once again, shapelets or prolate spheroidal wave functions could be a better choice in this case compared to clean components.

II. Shapelets

We shall present the use of Cartesian shapelets [5] as our orthonormal basis. Let (l, m) be the image plane coordinates (radians) and the Fourier plane coordinates be (u, v) in wavelengths. The image plane shapelet basis function can be given as

$$\phi_{n_1,n_2}(l,m,\beta) = \frac{1}{2^{n_1+n_2}\pi\beta^2 n_1! n_2!} H_{n_1}(l/\beta) H_{n_2}(m/\beta) \exp(-(l^2+m^2)/2\beta^2) \quad (1)$$

978-1-4244-6051-9/11/$26.00

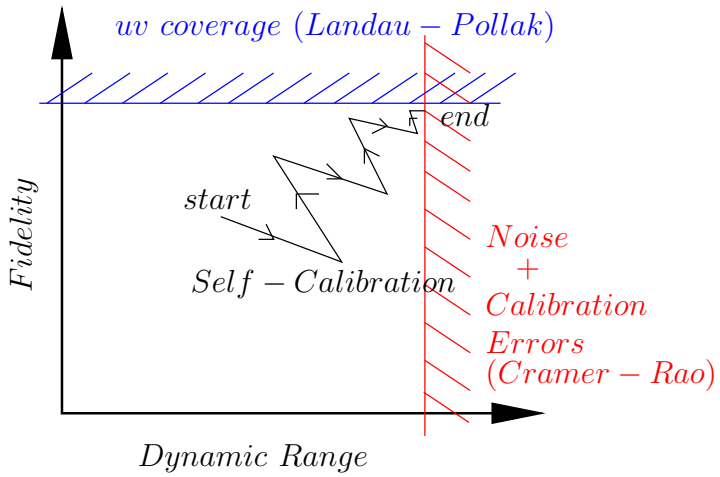

Fig. 1. The relationship between *fidelity* and *dynamic range* in a typical radio astronomical data reduction. The theoretical limits for fidelity is mainly given by the Landau-Pollak theorem. The dynamic range limits is mainly given by the Cramer-Rao lower bounds in calibration. A typical self-calibration involves stepwise improvement of dynamic range and fidelity until the limits are reached.

where β is the model scale. The model order is given by the integers n_1 and n_2. The Hermite polynomials are given as $H_{n_1}(l/\beta)$ and $H_{n_2}(m/\beta)$. The Fourier equivalent of $\phi_{n_1,n_2}(l,m,\beta)$ is $\phi_{n_1,n_2}(u,v,1/\pi\beta)$, within a scale factor.

Consider an image with L pixels that need not be on a rectangular grid and can have any arbitrary shape. Let $\mathbf{b}$ (size $L\times 1$) be the vectorized values of this image. Let M be the number of shapelet basis functions used (ideally should be no grater than N, the limit given by Landau-Pollak theorem). We construct matrix $\mathbf{P}$ (size $L\times M$) where each column is one basis function evaluated at the image grid points.

The basic steps needed to perform self calibration and imaging using this basis functions are:

1) Find model coefficients $\mathbf{m}$ (size $M\times 1$)
$$\mathbf{Pm}=\mathbf{b},\quad \widehat{\mathbf{m}}=\mathbf{P}^{\dagger}\mathbf{b} \tag{2}$$
where $\mathbf{P}^{\dagger}$ is the matrix pseudo inverse.
2) Let $\widetilde{\mathbf{P}}$ (size $D\times M$) be the Fourier equivalent of $\mathbf{P}$. The number of data points in the Fourier plane is D. Use $\widetilde{\mathbf{P}}$ to perform self-calibration and subtract the model from the calibrated data to get the residual $\widetilde{\mathbf{r}}$ (size $D\times 1$) as
$$\widetilde{\mathbf{r}}=\mathbf{z}-\widetilde{\mathbf{P}}\mathbf{m}. \tag{3}$$
where $\mathbf{z}$ (size $D\times 1$) is the calibrated data.
3) Use $\widetilde{\mathbf{r}}$ to make the residual image $\mathbf{r}$ and restore the model to get the updated image $\mathbf{c}$ as
$$\mathbf{c}=\mathbf{r}+\mathbf{Pm}. \tag{4}$$
4) If the limits of dynamic range and fidelity have not been reached, replace $\mathbf{b}$ with $\mathbf{c}$ and go back to step 1.

Note that in most of the steps described above, we do not explicitly construct any matrices or vectors. They are just used for notational convenience.

An example of a model construction using shapelets is given in Fig. 2 (a). In this figure, the top-left panel shows the original image used. Note that only the pixels above the noise floor is used in the model construction. The top-right panel shows the model coefficients. The bottom-left panel shows the error between the true image and the model. Finally, the bottom-right panel shows the model image.

It is noteworthy that the residual errors are prominent around the boundary of the source. The reason for this is that the shapelet basis functions are based on the Cartesian pixel grid. Therefore, for a source that can have any arbitrary shape, it is difficult to match the boundary contours. In principle, it is possible to find the right β and M and even shift the origin of the (l,m) coordinates to get the shapelet model with minimal error. However, this requires user experience and many trial and error iterations.

A way to overcome the shortcomings of shapelet basis functions (or any Cartesian basis function) is to use prolate spheroidal wave functions [11]. In Fig. 2 (b), we have shown some prolate spheroidal basis functions for the same source. Note that none of these basis functions have support beyond the perimeter of the source, thus creating fewer artifacts. However, the computation of prolate spheroidal wave functions is more expensive compared to shapelets.

We would like to point out that while finding the model coefficients in (2), it is sometimes better to do a rough deconvolution. This is done by convolving the columns of $\mathbf{P}$ by the point spread function (PSF), prior to estimating $\mathbf{m}$. An example of this

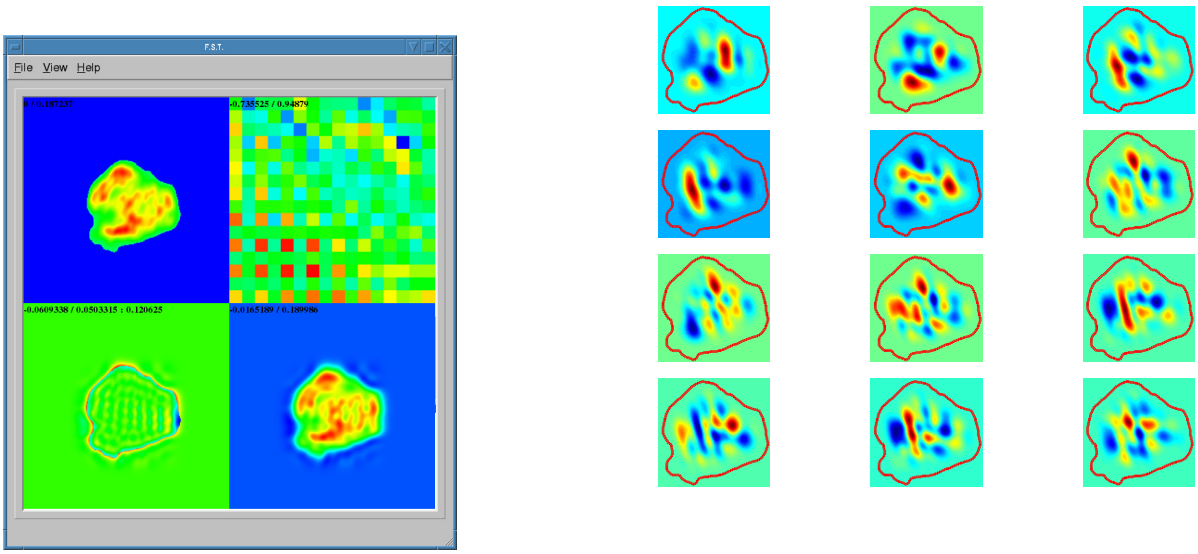

Fig. 2. (a) Shapelet decomposition of a source: (top-left) true image (top-right) model coefficients (bottom-left) residual image (bottom-right) model image. (b) Some prolate spheroidal wave functions for the same source. Note that the support of the prolate spheroidal wave functions always remain within the perimeter of the source, denoted by the dark line.

deconvolution is given in Fig. 3. The image on left in Fig. 3 is the image of which we wish to construct a shapelet model. However, we see that there are still some residual deconvolution errors. The image we used as the PSF is given in Fig. 3 middle panel. In this example, this is actually an image of a nearby point source. Once deconvolving with this approximate PSF, we get the image on right in Fig. 3. This deconvolved model is then used in the self-calibration and residual calculation steps.

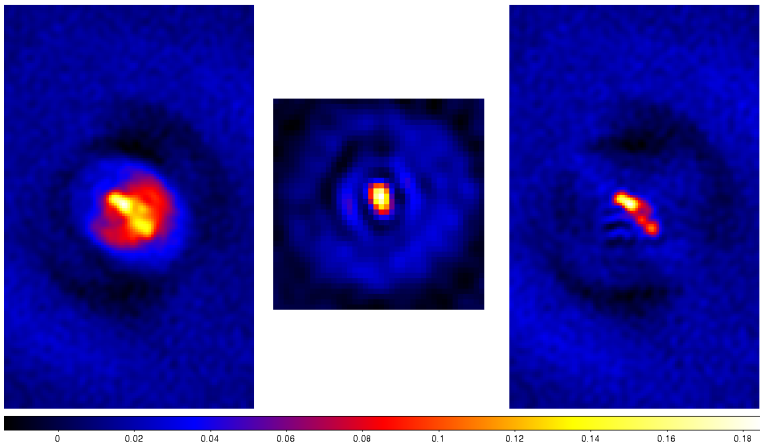

Fig. 3. Deconvolution of a source using shapelet basis: (left) true image (middle) image chosen as the point spread function (right) deconvolved image. The model based on the deconvolved image is used in calibration at later stages.

III. Results

We give an example of shapelet based imaging to improve the dynamic range of a Westerbork Synthesis Radio Telescope (WSRT) image of Taurus A at 117 MHz. Similar examples using shapelets and prolate spheroidal wave functions can be found in [2], [11]. In Fig. 4, the left panel shows the image obtained using conventional clean based techniques. The right panel shows the image obtained using a shapelet based model for the central source (Taurus A), which have been removed. It is clear that the artifacts caused by Taurus A on the left image have disappeared on the right image, giving a dynamic range of about 100 000.

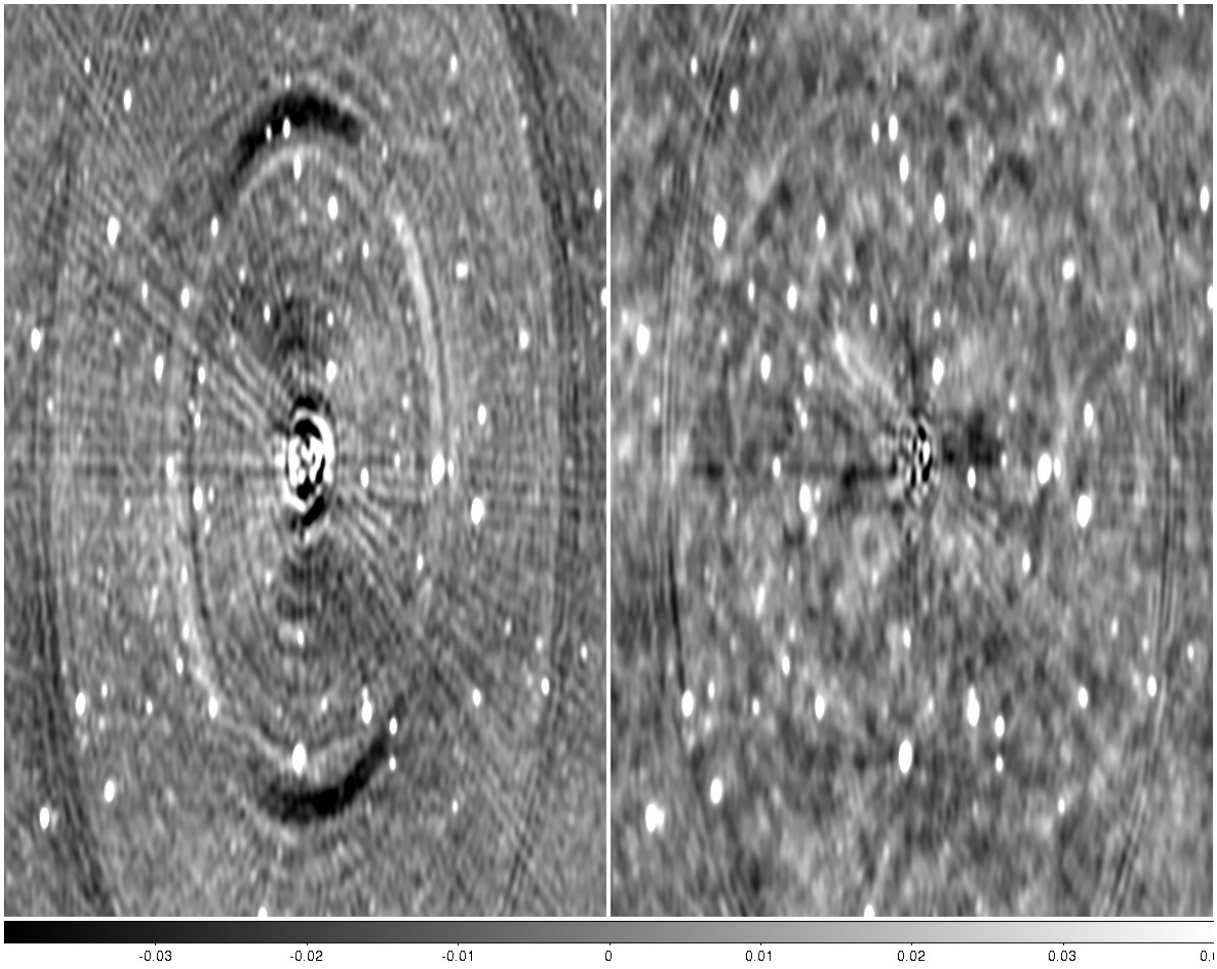

Fig. 4. WSRT images of Taurus A at 117 MHz. (left) Image obtained by conventional methods (right) Image obtained using shapelet based model for Taurus A. It is clear that the artifacts present on the left panel are gone on the right panel. This improves the dynamic range by one order of magnitude.

IV. Conclusions

We have presented the use of shapelets and prolate spheroidal wave functions in radio astronomical imaging to improve the dynamic range and image fidelity. We have also shown examples using real observations to verify our claim. Future work involves integration of these techniques to standard calibration and imaging packages and data processing pipelines.

V. Acknowledgment

We thank Ger de Bruyn, Wim Brouw, Ronald Nijboer, Michiel Brentjens, and Jan Noordam for comments and advise.

References

[1] D. Briggs, "High fidelity deconvolution of moderately resolved sources," Ph.D. dissertation, New Mexico Institude of Mining and Technology, 1995.
[2] S. Yatawatta, "Fundamental limitations of pixel based image deconvolution in radio astronomy," *in proc. IEEE Sensor Array and Multichannel Signal Processing Workshop (SAM), Israel*, pp. 69–72, 2010.
[3] J. Högbom, "Aperture synthesis with a non regular distribution of interferometer baselines," *A&A Suppl.*, vol. 15, pp. 417–426, 1974.
[4] T. Cornwell, "Multi-scale CLEAN deconvolution of radio systhesis images," *IEEE Trans. Sig. Proc.*, vol. 354, no. 199, pp. 42–55, 2004.
[5] A. Refregier, "Shapelets I. a method for image analysis," *MNRAS*, vol. 000, no. 1, pp. 42–55, 2001.
[6] R. Berry, M. Hobson, and S. Withington, "Modal decompositon of astronomical images with application to shapelts," *MNRAS*, vol. 354, no. 199, pp. 42–55, 2004.
[7] D. Slepian and H. O. Pollak, "Prolate spheroidal wave functions, Fourier analysis, and uncertainty-I," *Bell Syst. Tech. J.*, vol. 40, no. 2, pp. 43–61, 1961.
[8] H. J. Landau and H. O. Pollak, "Prolate spheroidal wave functions, Fourier analysis, and uncertainty-II," *Bell Syst. Tech. J.*, vol. 40, no. 2, pp. 65–84, 1961.
[9] M. C. H. Wright, "Image fidelity," *BIMA Memo 73*, 1999.
[10] D. Slepian, "On bandwidth," *Proc. of the IEEE*, vol. 64, no. 3, pp. 292–300, 1976.
[11] S. Yatawatta, "Radio astronomical image deconvolution using prolate spheroidal wave functions," *submitted to IEEE ICIP 2011*, 2011.
[12] S. J. Wijnholds and A. J. van der Veen, "Fundamental imaging limits of radio telescope arrays," *IEEE Jnl. on Sel. Areas of Sig. Proc.*, vol. 2, no. 5, pp. 613–623, 2008.